

Diurnal Cycle of Summer Precipitation over Subtropical East Asia in CAM5

WEIHUA YUAN,* RUCONG YU,⁺ MINGHUA ZHANG,[#] WUYIN LIN,[@] JIAN LI,[&]
AND YUNFEI FU**

* *LASG, Institute of Atmospheric Physics, Chinese Academy of Sciences, Beijing, China*

⁺ *LaSW, Chinese Academy of Meteorological Sciences, China Meteorological Administration, Beijing, China*

[#] *Institute for Terrestrial and Planetary Atmospheres, School of Marine and Atmospheric Sciences, Stony Brook University, Stony Brook, New York*

[@] *Brookhaven National Laboratory, Brookhaven, New York*

[&] *Chinese Academy of Meteorological Sciences, China Meteorological Administration, Beijing, China*

** *Laboratory of Satellite Remote Sensing and Climate Environment, School of Earth and Space Sciences, University of Science and Technology of China, Hefei, China*

(Manuscript received 27 February 2012, in final form 29 September 2012)

ABSTRACT

The simulations of summertime diurnal cycle of precipitation and low-level winds by the Community Atmosphere Model, version 5, are evaluated over subtropical East Asia. The evaluation reveals the physical cause of the observed diurnal rainfall variation in East Asia and points to the source of model strengths and weaknesses. Two model versions with horizontal resolutions of 2.8° and 0.5° are used.

The models can reproduce the diurnal phase of large-scale winds over East Asia, with an enhanced low-level southwesterly in early morning. Correspondingly, models successfully simulated the diurnal variation of stratiform rainfall with a maximum in early morning. However, the simulated convective rainfall occurs at local noontime, earlier than observations and with larger amplitude (normalized by the daily mean). As a result, models simulated a weaker diurnal cycle in total rainfall over the western plain of China due to an out-of-phase cancellation between convective and stratiform rainfalls and a noontime maximum of total rainfall over the eastern plain of China. Over the East China Sea, models simulated the early-morning maximum of convective precipitation and, together with the correct phase of the stratiform rainfall, they captured the diurnal cycle of total precipitation. The superposition of the stratiform and convective rainfalls also explains the observed diurnal cycle in total rainfall in East Asia. Relative to the coarse-resolution model, the high-resolution model simulated slight improvement in diurnal rainfall amplitudes, due to the larger amplitude of stratiform rainfall. The two models, however, suffer from the same major biases in rainfall diurnal cycles due to the convection parameterization.

1. Introduction

The diurnal cycle is one of the most fundamental modes of variability of the global climate system, and the regular occurrence of precipitation at a particular time of the day is connected with both regional and large-scale dynamical and thermal conditions (Yang and Slingo 2001; Sorooshian et al. 2002). Large differences exist in the diurnal variations between the open oceans and the continents (e.g., Dai 2001). Oceanic deep convection tends to reach its maximum in the early morning

(Kraus 1963; Andersson 1970; Gray and Jacobson 1977; Randall et al. 1991) and continental convection generally peaks in the late afternoon (Cook 1939; Wallace 1975; Hamilton 1981). Moreover, affected by the complex land–sea and mountain–valley breezes, significant regional variations over the continents have been reported (Yang and Slingo 2001; Kikuchi and Wang 2008). The rainfall diurnal cycle over land can be explained by the thermodynamic processes that affect the surface temperature and vertical static stability and by the dynamical processes affecting convergence in the boundary layer or the long nocturnal life cycle of mesoscale convective systems (Wallace 1975; Oki and Musiak 1994; Yang and Slingo 2001; Nesbitt and Zipser 2003). The cause for the observed diurnal cycle of precipitation

Corresponding author address: Rucong Yu, China Meteorological Administration, National Climate Center, 46 Zhongguancun Nandajie, Beijing 100081, China.
E-mail: yrc@lasg.iap.ac.cn

over the open ocean remains debatable. As summarized by Nesbitt and Zipser (2003), theories generally fall into three categories: the differential radiative heating between the convective and surrounding cloud-free region (Gray and Jacobson 1977); the absorption of shortwave radiation by the upper portions of the convective anvils during day and longwave cooling at cloud top during night, which influence stability and relative humidity (Randall et al. 1991); and a more complex mechanism that is linked to the daily variations in the surface layer over the ocean (Dai 2001).

The ability to correctly simulate the diurnal cycle of precipitation provides an important test of global climate models (GCMs), from radiative transfer and surface exchanges to boundary layer, convective, and cloud processes (Lin et al. 2000; Xie and Zhang 2000; Yang and Slingo 2001; Zhang 2003; Collier and Bowman 2004; Lee et al. 2007b; Sato et al. 2009). However, simulations of the diurnal cycles of the hydrological processes are still big challenges for GCMs (Betts and Jakob 2002a; Collier and Bowman 2004; Dai and Trenberth 2004; Dai 2006). Diurnal precipitation in GCMs is typically too strong, peaks too early over major landmasses, and is too horizontally homogenous relative to observations (Collier and Bowman 2004). They usually fail to adequately capture the observed early morning peak over the oceans and the nocturnal peak and the propagating signals over the eastern slope of the elevated land areas. High-resolution models have been shown to improve the behavior of the diurnal precipitation in certain regions, such as over the Maritime Continent and Bay of Bengal, and the initiation and downslope propagation of moist convection over the Rockies and the adjacent Great Plains (Arakawa and Kitoh 2005; Lee et al. 2007b; Ploshay and Lau 2010). However, large errors in both the phase and amplitude of the precipitation diurnal cycle remain even in the high-resolution GCMs in other regions. The discrepancies between simulations and observations have not been fully understood, which could be associated with the failure in capturing the growth of the nonprecipitation convective boundary layer (Betts and Jakob 2002b,a) and unrealistically strong coupling of convection to surface heating (Lee et al. 2007a; Hara et al. 2009; Ploshay and Lau 2010).

The diurnal cycles of rainfall over subtropical East Asia have distinct characteristics with considerable regional features (Yu et al. 2007; Chen et al. 2009; Yin et al. 2009; Yuan et al. 2012). Over southern inland China, summer rainfall peaks in the late afternoon. Over the Tibetan Plateau, the rain gauge data exhibit midnight diurnal peaks, while the rainfall in satellite data usually reaches the maximum in late afternoon. This inconsistency may be caused by the phase differences of

diurnal rainfall variation in valleys and over the mountains, with rain gauges capturing diurnal variation in the valleys and satellites capturing that over the mountains (Chen et al. 2012; Yuan et al. 2012). Rainfall in southwestern China presents primarily midnight and early-morning diurnal peaks. In central eastern China, the regionally averaged rainfall in station data has two comparable diurnal peaks, one in late afternoon and the other in early morning. The observed diurnal rainfall provides an ideal test bed for model parameterizations. The objective of this paper is to evaluate the performance of the Community Atmospheric Model, version 5 (CAM5), in simulating the diurnal variation of rainfall over subtropical East Asia by using rain gauge and satellite data, as well as the causes of the success and failure of the models. To study the resolution dependence of our results, we used two versions of the model with different resolutions.

Section 2 describes the models, experiments, and datasets. Section 3 presents the summer mean precipitation and low-level wind simulations. Section 4 shows the diurnal features of total rainfall over subtropical East Asia. Section 5 further discusses the diurnal variation of convective and stratiform rainfall and the influence of large-scale forcing. Section 6 summarizes the results.

2. Model and data description

The model used in this study is CAM5, the atmospheric component of the Community Earth System Model (CESM). CAM5 (Neale et al. 2010) includes substantially revised physical parameterizations over CAM3 and CAM4 (Collins et al. 2004; Collins et al. 2006). CAM5 contains an updated moist boundary layer scheme (Bretherton and Park 2009), cumulus convection scheme (Neale et al. 2008), shallow cumulus convection scheme (Park and Bretherton 2009), stratiform cloud microphysics scheme (Morrison et al. 2005; Morrison and Gettelman 2008; Gettelman et al. 2010), radiation scheme (Iacono et al. 2008), liquid cloud macrophysical closure, and interactive aerosols (Neale et al. 2010).

The deep convection parameterization in CAM3 is a bulk mass flux approach described in Zhang and McFarlane (1995, hereafter ZM). Closure in the ZM scheme is achieved by a rate limitation on the consumption of convective available potential energy (CAPE). The default implementation of ZM uses a traditional definition of CAPE, which is calculated using an air parcel ascending pseudoadiabatically and not mixing with the environment and is known to unrealistically bias the near-surface thermodynamic conditions and be relatively insensitive to the free-tropospheric humidity, particularly on subdiurnal time scales (Donner and Phillips 2003).

The new closure of the deep convection scheme used in CAM5 (Neale et al. 2008) allows mixing of the air parcel with environmental air depending on an assumed entrainment rate (Raymond and Blyth 1986, 1992). This calculation makes the CAPE sensitive to the moisture profile above the boundary layer. The modification of the CAPE has a significant impact on the frequency and strength of convective events generated by the ZM scheme (Neale et al. 2008).

The simulations analyzed in this study are 5-yr continuous integrations driven by monthly mean climatological sea surface temperatures and using a spectral dynamical core. Only results of the last four summers (June–August) are shown. The simulations are carried out at both coarse ($\sim 2.8^\circ$) and high ($\sim 0.5^\circ$) horizontal resolutions with 30 vertical levels.

The model output is compared with observational counterparts based on datasets provided by station rain gauges, Tropical Rainfall Measuring Mission (TRMM) 3B42 and 2A25, and the Climate Forecast System Reanalysis (CFSR) from 1998 to 2006.

Hourly rain gauge data from 394 stations used in this study were collected, compiled and quality controlled by the National Meteorological Information Centre of the China Meteorological Administration (Yu et al. 2007). Further quality control as described in Yuan et al. (2012) has also been applied.

The TRMM 3B42 precipitation data (3-hourly, 0.25°) (Huffman et al. 2007) were created by blending passive microwave data collected by the TRMM Microwave Imager (TMI), the Special Sensor Microwave Imager, the Advanced Microwave Scanning Radiometer for Earth Observing System, the Advanced Microwave Sounding Unit B, and the infrared (IR) data collected by the international constellation of geosynchronous earth orbit based on calibration by the precipitation estimate of the TMI and Precipitation Radar (PR) combined algorithm. A gauge correction was applied over land (Huffman et al. 2007).

The rainfall in TRMM PR data (product 2A25) is classified into three types: convective, stratiform, and “other” (Iguchi et al. 2000). Simply, a stratiform profile is classified if PR detects a bright band near the freezing level in the profile. If no bright band exists and any value of radar reflectivity in the beam exceeds 39 dBZ, the profile is named as convective. Exceptions to both convective and stratiform are labeled as other in the dataset. Over subtropical East Asia, the convective and stratiform rainfall is more than 90% of total rainfall amount.

The CFSR is employed to describe the large-scale circulations. CFSR was recently developed at the National Centers for Environmental Prediction (Saha et al. 2010). It is the first reanalysis in which the guess fields

are taken as the 6-h forecast from a coupled high horizontal atmosphere–ocean climate system with an interactive sea ice component.

Four subregions are defined, following Yuan et al. (2012), based on the different underlying surface types or elevations and diurnal features. They are the Tibetan Plateau (TP), defined to be the most elevated region ($28^\circ\text{--}35^\circ\text{N}$, $90^\circ\text{--}100^\circ\text{E}$) with mean elevation of 4452 m; the western plain ($28^\circ\text{--}35^\circ\text{N}$, $103^\circ\text{--}109^\circ\text{E}$) and eastern plain ($28^\circ\text{--}35^\circ\text{N}$, $112^\circ\text{--}120^\circ\text{E}$) with mean elevations of 1203 and 135 m and different diurnal variations; and the East China Sea ($28^\circ\text{--}35^\circ\text{N}$, $122^\circ\text{--}130^\circ\text{E}$). These domains are marked in Fig. 1a. The diurnal amplitudes of rainfall are calculated as

$$A = \frac{R_{\max} - \bar{R}}{\bar{R}} \times 100\%,$$

where R_{\max} is the maximum of rainfall and \bar{R} is the mean value. Rainfall diurnal variation is normalized as

$$D(h) = \frac{R(h) - \bar{R}}{\bar{R}},$$

where $D(h)$ is the rainfall after normalization and $R(h)$ is the original (Yu et al. 2007).

3. Summer mean precipitation and low-level circulation

Before evaluating the diurnal cycle of precipitation, the summer mean rainfall amount and 850-hPa winds in observations and model simulations are compared in Fig. 1.

Figure 1a shows the summer mean rainfall amount over East Asia derived from TRMM 3B42. Maximum rainfall is near the southern border of China, along the Yangtze River, and over the Korean Peninsula. The locations of these maxima correspond to two rain belts. One, known as the subtropical mei-yu/baiu front, exhibits zonally elongated heavy rainfall centers along the Yangtze River ($100^\circ\text{--}120^\circ\text{E}$) near 30°N toward the southern part of the Korean Peninsula. The other is located along the southern slope of the Himalayas to the South China Sea (around 20°N), which is influenced by the Asian monsoon and topography.

The rainfall distribution is closely related to the large-scale atmospheric circulation. In the lower troposphere, southwesterlies prevail over southeastern China. The wind speed significantly decreases around 30°N . A cyclonic circulation is located over the western plain. The combination of the southwest vortex and the low-level convergence of warm tropical water vapor provide a favorable

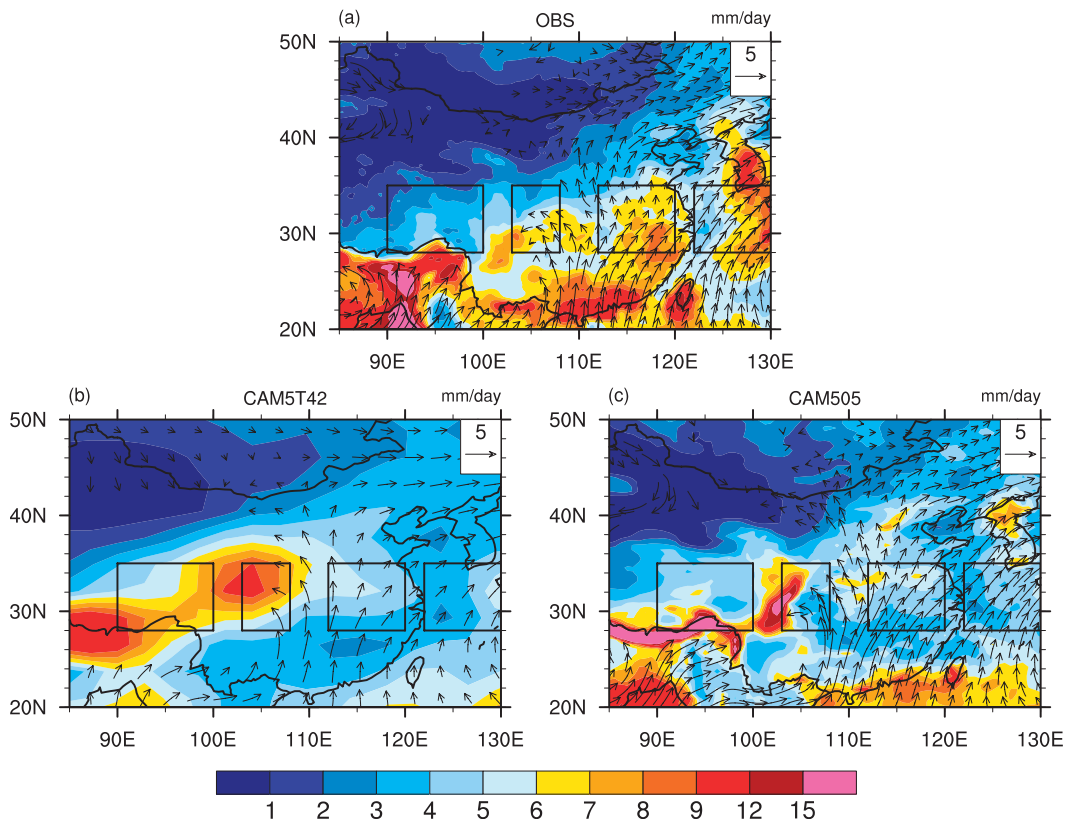


FIG. 1. Summer (June–August) mean precipitation (mm day^{-1}) and 850-hPa wind fields (m s^{-1}) in (a) TRMM 3B42 and the CFSR, (b) the coarse-resolution model (CAM 5T42), and (c) the fine-resolution model (CAM 505). Four subregions are outlined as the Tibetan Plateau (TP), the western plain, the eastern plain, and the East China Sea.

environment for maintaining the rainfall systems along the Yangtze River (Tao and Chen 1987; Zhou et al. 2005).

CAM5 with both resolutions (Figs. 1b,c) simulated the overall distribution of mean precipitation, with wet conditions at the southern and eastern slopes of the plateau and in the Yangtze River valley and dry conditions in northwestern China. The spatial correlation coefficient between the coarse-resolution (fine-resolution) model simulation and 3B42 is 0.5 (0.6). There are two common biases, however. One is that the models simulated little rain over South China; the second is that the simulated monsoon rainbands over the Yangtze River valley are located too far to the north, resulting in too much rainfall over North China.

Compared with the coarse-resolution model version (Fig. 1b), the fine-resolution model (Fig. 1c) improved the precipitation simulation in several aspects: 1) the maximum rainfall centers along the edges of TP are much improved, reflecting the benefit of resolving the topography better in the fine-resolution model; 2) the rain belt over the ocean along 20°N is

more realistic; and 3) the maximum rainfall over the Korean Peninsula is much improved. As a result, the regional ($20^{\circ}\text{--}50^{\circ}\text{N}$, $85^{\circ}\text{--}130^{\circ}\text{E}$) averaged rainfall amount in the high-resolution model (4.28 mm day^{-1}) is closer to the observation (4.31 mm day^{-1}) than that in the coarse one (3.91 mm day^{-1}).

Both versions of the CAM5 simulated the 850-hPa winds that are generally consistent with the observation. They reproduced the southwesterlies over southeastern China and the cyclonic circulation over the western plain. Despite these successes, however, both models overestimated the magnitude of the wind over southeastern China. They did not capture the decrease of wind speed near the Yangtze River, as seen in the CFSR (Fig. 1a). This is consistent with biases in the rainfall distribution that extend too far to the north in the models. Additionally, we find that the high-resolution model exhibits a larger overestimation in wind speed (0.51 m s^{-1}) than that in the coarse-resolution model (0.40 m s^{-1}) over land, although it simulates wind speed over the ocean better. The causes of these sensitivities to resolution are yet to be understood.

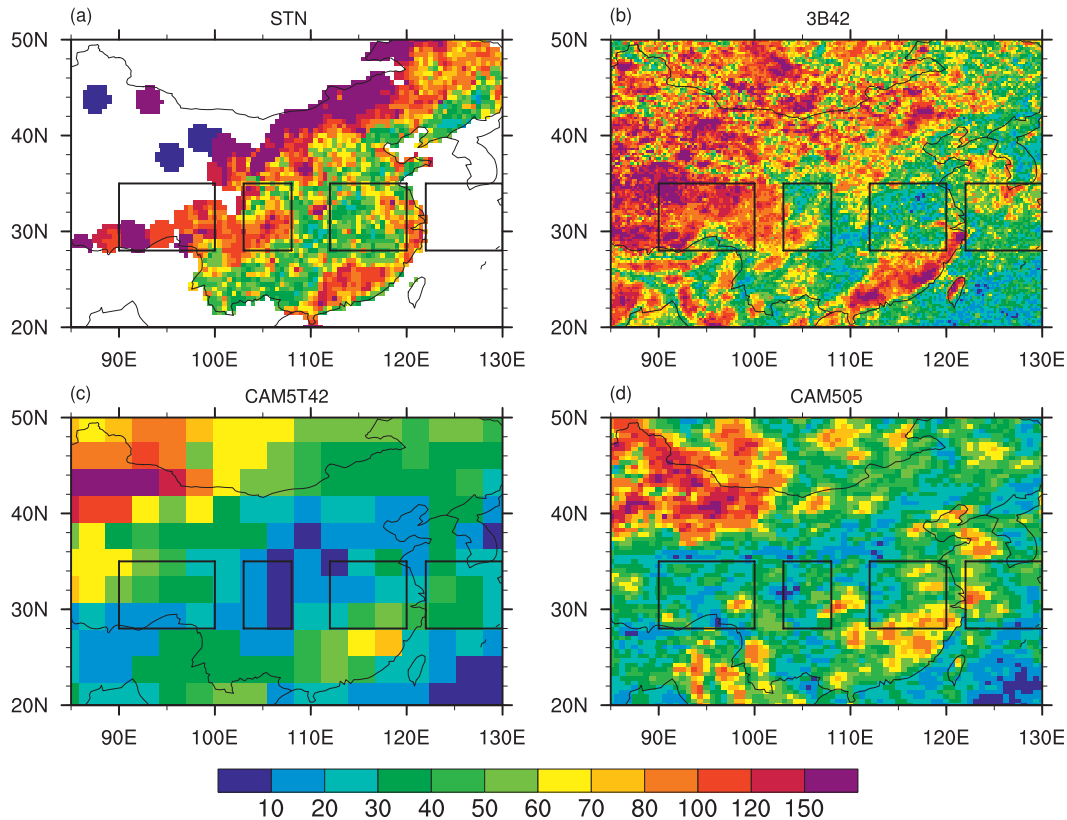


FIG. 2. Amplitudes of rainfall diurnal variations (%) derived from (a) station rain gauge data, (b) TRMM 3B42, and simulations of the (c) coarse and (d) fine-resolution model. Four subregions are outlined.

4. Diurnal cycle of precipitation

Figure 2 shows the distribution of the amplitudes, in terms of percentage to daily-mean rainfall, of the diurnal rainfall in the observations and models. The two observational datasets from station rain gauges (Fig. 2a) and 3B42 (Fig. 2b) are generally consistent with each other over land. Maximum diurnal variations are located along the coastal land regions of South China and in northwestern China, the Tibetan Plateau, and the western plain. The TRMM data also show large diurnal rainfall amplitudes over the East China Sea.

CAM5 generally captured the spatial pattern of the amplitude distributions, including large values over the coastal land regions in South China, over northwestern China, and the East China Sea; the spatial correlation coefficients between the 3B42 and simulations both exceed 0.4. However, the models underestimated the values of the amplitudes, especially over the TP and western plain. Between the two models, the high-resolution CAM5 simulated overall larger diurnal amplitudes, closer to the observations.

Figure 3 shows the normalized rainfall as a function of local solar time (LST) in both observations and in the

models for the four selected regions with distinctive rainfall diurnal phases (Yuan et al. 2012). Yuan et al. pointed out that the diurnal variations from rain gauges (gray solid lines) and TRMM (gray dashed lines) are generally consistent with each other except over the TP. This inconsistency was caused by the phase differences of diurnal rainfall variation in valleys and over mountains, with rain gauges capturing the diurnal variation in the valleys and satellites capturing it over the mountains (Yuan et al. 2012; Chen et al. 2012). Over the eastern and western plains, the nocturnal rainfall in 3B42 is relatively underestimated, consistent with Zhou et al. (2008) and Yuan et al. (2012). As the rain gauge measured the surface precipitation directly, the density of rain gauges is large, and the passive microwave detection tends to overestimate rainfall occurring in the afternoon (Sorooshian et al. 2002; Yuan et al. 2012), we adopt the results in station data are more reliable over these two regions. Over the East China Sea, there are only several island stations, and the passive microwave measurements are more reliable over the oceans (Kummerow et al. 2001), so we use 3B42 as the observation data for this region. In Fig. 3, we therefore use both the rain gauge

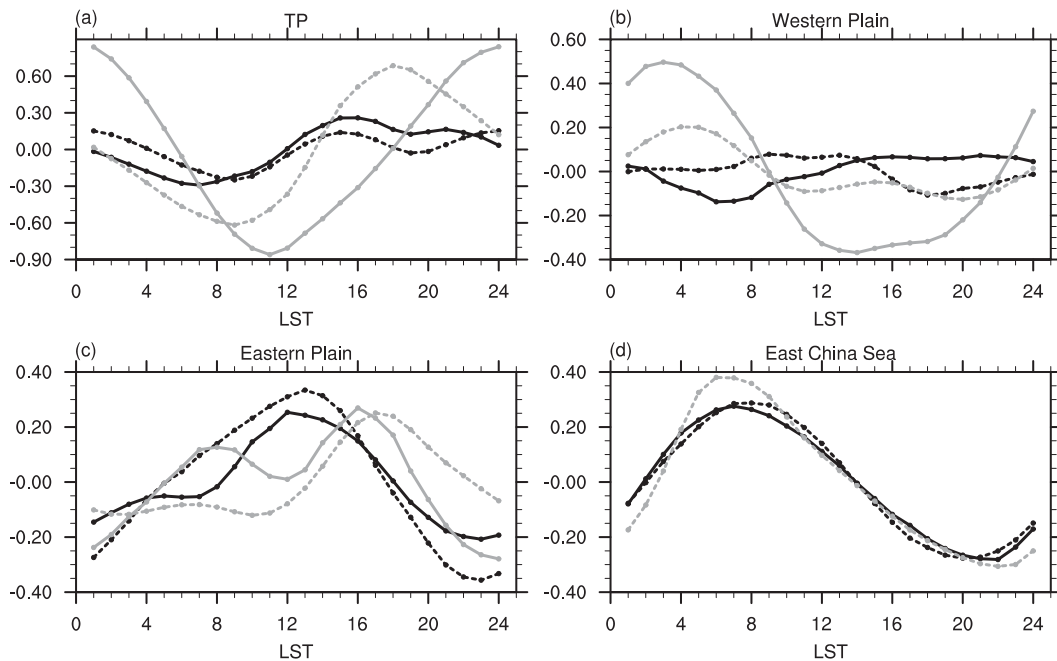


FIG. 3. Normalized (by daily mean) diurnal variations of summer precipitation averaged for (a) the TP, (b) western plain, (c) eastern plain, and (d) the East China Sea outlined in Fig. 1 from station observations (gray solid lines), TRMM 3B42 (gray dashed lines), the coarse-resolution model (black solid lines), and the fine-resolution model (black dashed lines). The x axis is LST.

data and 3B42 as observations for the TP but use rain gauge data for the western and eastern plains and satellite data for the East China Sea.

Figure 3a shows that over the TP satellite data shows a clear late-afternoon diurnal maximum, while rain gauge data shows a distinct midnight diurnal maximum. In the models, however, the diurnal amplitudes are much smaller. The peak of the coarse-resolution model is in the afternoon, earlier than either one of the observations, and the primary peak of the fine-resolution model is closer to that in the station data. For the western plain, Fig. 3b shows a distinct early-morning diurnal peak in observation. The models, however, simulated much smaller diurnal amplitudes than those in observations. The diurnal phase of the coarse-resolution model is almost out of phase with observation, and the higher-resolution model is somewhat better in the diurnal phase. The observed rainfall over the eastern plain (Fig. 3c) presents diurnal variations with two maxima at 1600 and 0800 LST, respectively. Both coarse- and high-resolution models simulated the diurnal rainfall variation with comparable amplitudes but with the diurnal maximum occurring at local noontime. Over the East China Sea the observation in Fig. 3d shows a clear diurnal peak in early morning. The two models both simulated the diurnal phase correctly with significant amplitudes. This is a

remarkable performance of the model because it is well known that climate models generally simulate a too weak diurnal cycle over the oceans (Collier and Bowman 2004; Dai and Trenberth 2004).

In Fig. 4, we show the homograph diurnal rainfall averaged between 28° and 35° N as a function of longitude. In observations (Figs. 4a,b), there is an eastward-propagating signal of the diurnal rainfall from the TP to the western plain (from 100° to about 113° E). As mentioned earlier, over the TP, the diurnal maximum in station data occurs at midnight, later than the evening maximum in the satellite data. As a result, the propagation speed is slower in the station data (Fig. 4a) than that in the satellite data (Fig. 4b). The coarse-resolution CAM5 (Fig. 4c) misses this propagating signal; the high-resolution CAM5 (Fig. 4d) captures the propagating signal but with weaker amplitudes. Over the eastern plain, the simulated diurnal maximum occurs about 3 h earlier. The two simulations both well capture the phase shift around the coastline. These are consistent with the comparison in Fig. 3 for the four selected regions.

5. Convective versus stratiform rainfall

To understand the diurnal behavior of the models relative to observations, we further examine convective

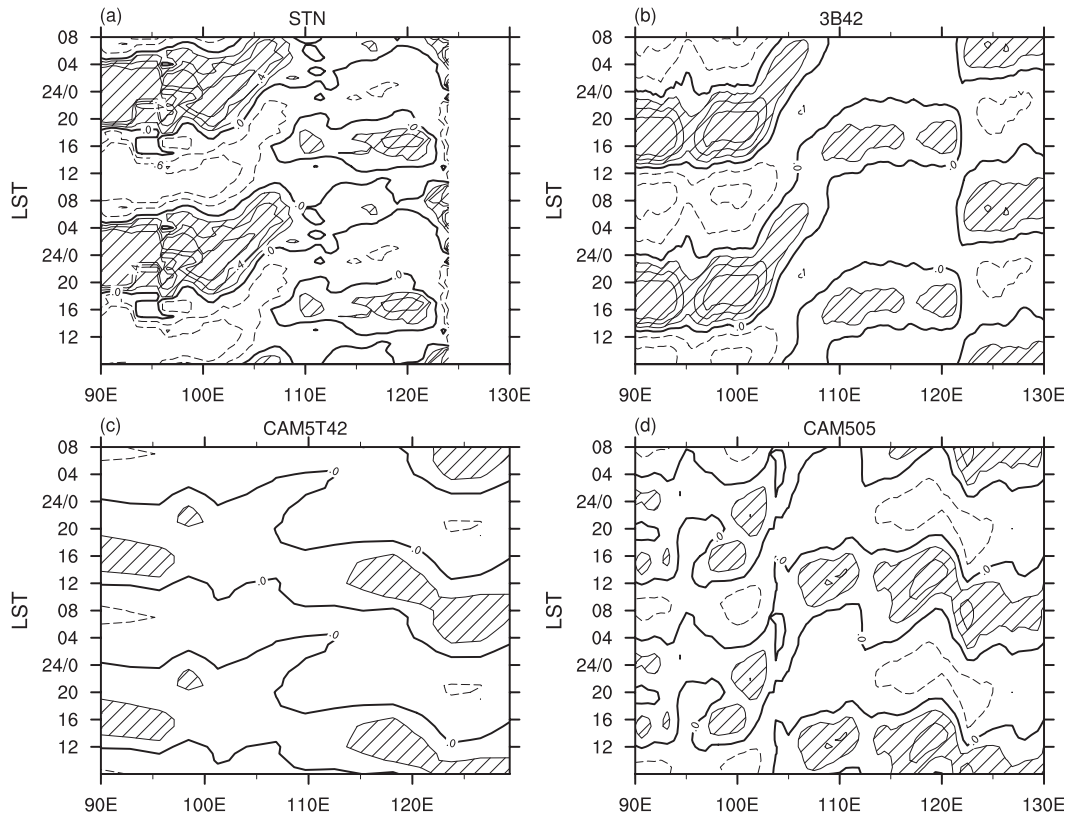


FIG. 4. Time-longitude distributions of the normalized (by daily mean) rainfall diurnal variation averaged between 28° and 35°N derived from (a) station rain gauge data, (b) TRMM 3B42, (c) the coarse-resolution model, and (d) the fine-resolution model. The y axis is LST.

and stratiform precipitation separately. Convective rainfall in the model is generated by the deep and shallow convective schemes as a result of convective instability, while the stratiform rainfall is formulated in the large-scale precipitation scheme due to saturation condensation within stratiform clouds. We will compare the diurnal variations of convective and stratiform rainfall in the simulations with the results in TRMM 2A25. As there may be uncertainties in the definition of the convective and stratiform rainfall in TRMM 2A25, we used the heavy and moderate/weak rainfall in station data for validation, following Dai (2006). Heavy rainfall is defined as rainfall greater than 9.4 mm h^{-1} , which is the 95th percentile rainfall intensity over the area within 28° – 35°N , 103° – 125°E . As shown in Fig. 6a, the ratio of moderate/weak and heavy rainfall in station data are generally consistent with that of convective and stratiform rainfall in 2A25: the moderate/weak rainfall dominates over the western plain; the ratio of the two kinds of rainfall are comparable over the eastern plain; and the results of data on some island stations also are similar as those in 2A25 over the East China Sea. The consistency of the two data

gives us confidence to use the 2A25 products in the evaluation. Because of the different diurnal features in the satellite data and rain gauge over the TP as shown earlier and the uncertainty of rainfall classification into convective and stratiform over the TP in 2A25 (Fu and Liu 2007), we will exclude the TP in the following analysis. We hope to revisit the TP region when more observations become available.

Figure 5 shows the diurnal cycle of convective (left column) and stratiform rainfall (right column) over the western plain (top row), eastern plain (middle row), and the East China Sea (bottom row) in both observations and two simulations. Since we normalized the diurnal variation relative to the daily mean, the impact of the different definitions of precipitation type between the models and TRMM on the comparison is minimized.

A remarkable feature in Fig. 5 is the overall consistency of diurnal stratiform precipitation in observations and model simulations for all three regions. For convective precipitation, the models did not do as well. Both models simulated large amplitudes and near noontime peaks in the western and eastern plains with a minimum

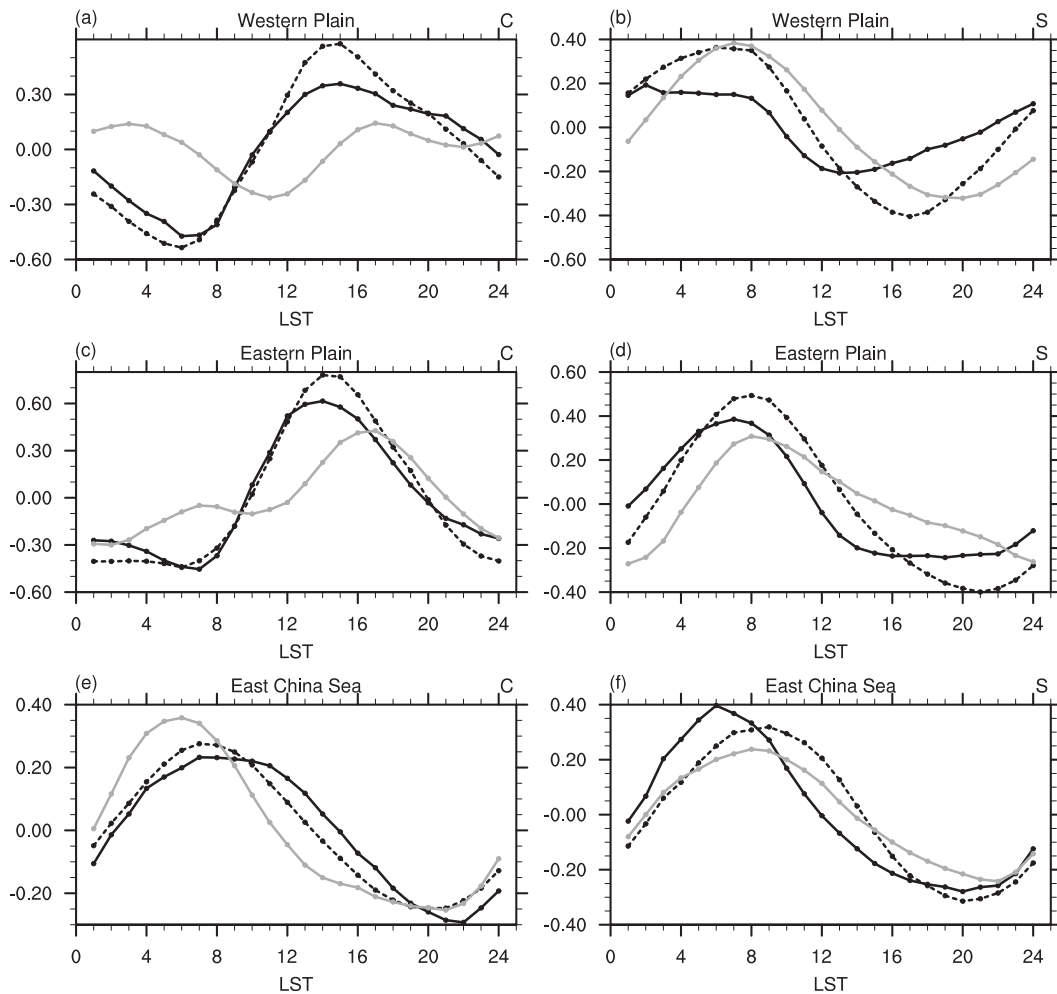


FIG. 5. Normalized (by daily mean) diurnal variations of summer (left) convective and (right) stratiform precipitation averaged in (top) the western plain, (middle) the eastern plain, and (bottom) the East China Sea outlined in Fig. 1 derived from TRMM 2A25 (gray lines), the coarse-resolution model (black solid lines), and the fine-resolution model (black dashed lines). The x axis is LST.

in early morning. However, in observations, the amplitude of convective rainfall is much smaller and there are two diurnal peaks in early morning and late afternoon over the western plain; the phase of the eastern plain is similar to that in the western plain, but the late-afternoon peak is more pronounced. Over the ocean, the simulated diurnal convective precipitation is better. There is a slight delay (3 h) in the precipitation maximum in early morning and some underestimation of the amplitude, but the overall features in the models agree with the observations. Comparing the two versions of the model, we can find that the high-resolution model has larger amplitude in both stratiform and convective components. There is no systematic advantage of the high-resolution model in simulating the amplitude and diurnal phase of the two rainfall components.

Figures 5a,b together show that, over the western plain, the observed convective maximum in the early morning is in phase with the stratiform maximum, but the second observed convective maximum in late afternoon is in opposite phase with the stratiform rainfall. The sum of the convective and stratiform diurnal rainfall, after weighting by their respective daily means, gives rise to the total diurnal rainfall. The percentages of the daily means of the convective and stratiform rainfall to the total amount as a function of longitude are shown in Fig. 6. It is seen that, over the western plain, the stratiform component is several times larger than the convective component. As a result, the total diurnal rainfall primarily follows the stratiform component with an early-morning peak as in Fig. 3b. In the models, Figs. 5a,b also show that, over the western plain, the diurnal phase of the

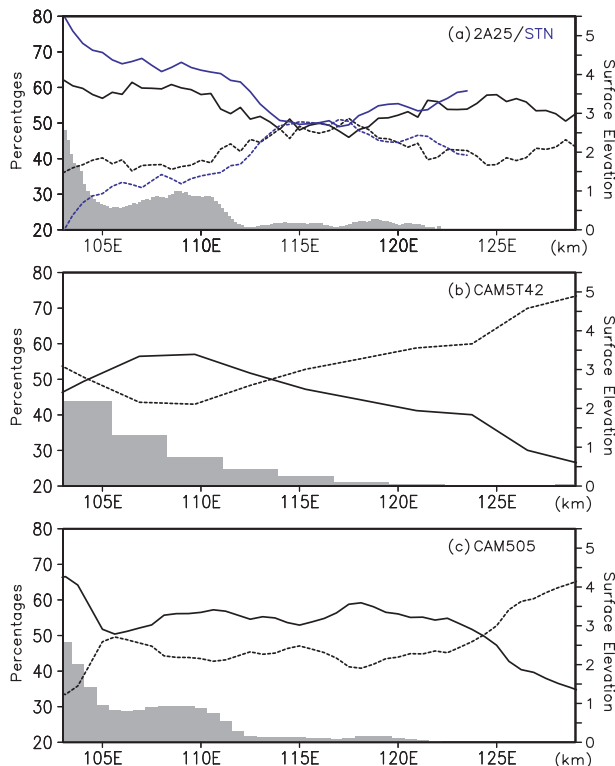


FIG. 6. Percentage of (left axis) convective (dashed black lines) and stratiform (solid black lines) rainfall amount to total rainfall amount averaged between 28° and 35°N derived from (a) TRMM 2A25, (b) the coarse-resolution model, and (c) the fine-resolution model. Blue lines in (a) are the percentages (left axis) of heavy rainfall amount (dashed) and moderate/weak (solid) rainfall amount to total rainfall amount averaged between 28° and 35°N derived from station data. The gray bars represent the surface elevations (km) averaged between 28° and 35°N (right axis).

convective rainfall is roughly opposite to the diurnal phase of the stratiform rainfall. Furthermore, Figs. 6b,c show that the percentages of the daily-mean convective rainfall in the models are comparable to those of the stratiform rainfall. As a result, there is a large out-of-phase cancellation of diurnal variation between the convective and stratiform components in the models, leading to much smaller simulated amplitude as shown in Fig. 3b. The simulated stratiform rainfall percentage in the high-resolution model is larger than that in the coarse one over the western plain. This explains why the diurnal phase of total rainfall in the high-resolution model is better (Figs. 3b, 4).

Over the eastern plain, the results are overall similar to those over the western plain in terms of the phase relationship in both observation and the two models but with the following differences: 1) the observed convective maximum in the late afternoon is more pronounced

than that in the early morning and 2) the observed stratiform minimum occurs at midnight rather than late afternoon. These two features, together with the comparable percentages of daily-mean convective and stratiform rainfall (Fig. 6a), lead to the two-peak diurnal rainfall with a dominant late-afternoon maximum discussed earlier. In the models, the simulated convective diurnal amplitude is much larger than the observation and larger than the diurnal amplitude of the stratiform rainfall. These explain the dominant noontime diurnal total rainfall in the models shown in Fig. 3c.

The convective and stratiform rainfall are diurnally in phase with each other in observations over the East China Sea, and the models approximately captured the observations. As a result, even though the percentage of the daily convective rainfall over the ocean is overestimated in the models (Figs. 6b,c), the partition does not affect the phase of the diurnal variation of total rainfall. This explains the remarkable success of the models in simulating the diurnal rainfall in Fig. 3d.

Therefore, failure of the models in simulating the diurnal variation of total rainfall over the western and eastern plains is primarily due to the diurnal convective precipitation. It is too strong and occurs too early in the day. It offsets the diurnal variation of stratiform precipitation. The success of the models is due to their ability to simulate the diurnal stratiform rainfall. Success of the models over the ocean is because the convective and stratiform precipitation is diurnally in phase, with an early-morning maximum. The slight improvement of the high-resolution model over the coarse-resolution model in the western plain is because it simulated a larger diurnal amplitude of stratiform rainfall and larger ratio of stratiform to convective precipitation, which is consistent with previous studies (Duff et al. 2003; Boyle and Klein 2010).

Climate models are known to simulate maximum convection around noontime when they use a closure of the CAPE in its cumulus parameterizations (Xie and Zhang 2000; Xie et al. 2002; Dai and Trenberth 2004). Over land, CAPE typically reaches maximum around noontime. Although the dilute CAPE used in CAM5 has involved the effect of environmental air, the convection in the model still responds to CAPE instantaneously and the simulated convective rainfall reaches maximum near noontime. In observations, however, convective systems have life cycles, so the convective activity could be delayed, which is seen over the western and eastern plains. Over the East China Sea maximum convection occurs in early morning, which is also in phase with the diurnal variation of CAPE in both simulations (figures omitted).

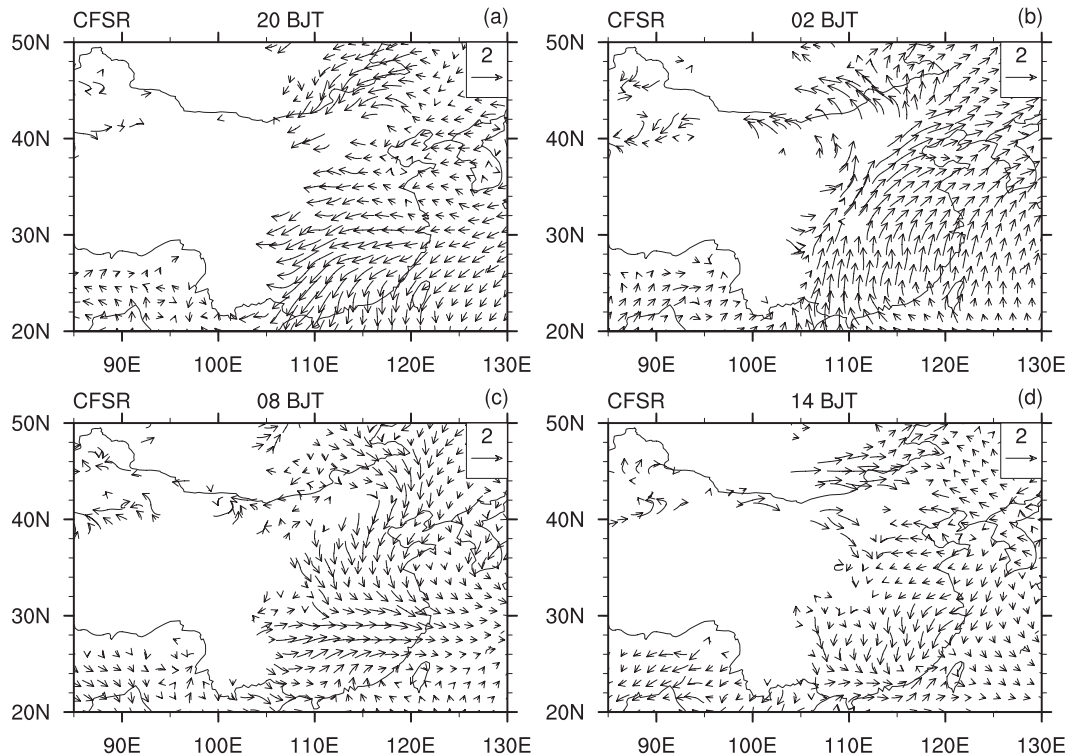


FIG. 7. Summer mean of 850-hPa wind anomalies (minus daily mean, m s^{-1}) at (a) 2000, (b) 0200, (c) 0800, and (d) 1400 BJT in the CFSR reanalysis.

To understand the diurnal phase of the stratiform rainfall and why the models are able to simulate the observations, we show in Fig. 7 the evolution of the diurnal component of low-level winds at 2000, 0200, 0800, and 1400 Beijing time (BJT) from CFSR data. At 2000 BJT (Fig. 7a), the anomalous winds are toward the plateau. During midnight (Fig. 7b), a southwesterly anomaly dominates most of mainland China, strengthening the low-level southwesterly jet shown in Fig. 1a. In the next 6 h (0800 BJT, Fig. 7c), the low-level wind has a southwesterly anomaly over southern China and a northwesterly one north of the Yangtze River valley. In the afternoon (1400 BJT), the northerly anomaly dominates most of subtropical East Asia (Fig. 7d). As a result, the low-level southwesterly shown in Fig. 1a is greatly weakened at this time. This change of the diurnal variation of low-level winds is consistent with the nighttime low-level jet that also occurs over the southern Great Plains of the United States. It is believed to be caused by the diurnal thermodynamic difference related with the terrain. The above diurnal variation of the 850-hPa winds corresponds to early-morning convergence in the low troposphere for the western and eastern plains and the East China Sea (as shown in Fig. 10; gray lines with open circles). These can explain the

maximum early-morning stratiform precipitation in all three regions.

The two CAM5 simulations (Figs. 8 and 9) both reproduced consistent clockwise rotation of the diurnal wind fields as in the reanalysis (Fig. 7). At 2000 BJT, the anomaly wind blows toward the plateau. The southwesterly strengthens over subtropical East Asia at 0200 BJT. During the morning, a convergence zone can also be found in both simulations but is located south of that in the observation. In the afternoon, the anomalous winds in the simulations also blow against the summer mean flow, weakening the southwestern monsoon airflow shown in Fig. 1. However, the magnitude in the models is larger than that in the observation. For the divergence over the three regions (Fig. 10), the two simulations also well captured the diurnal variations revealed by the reanalysis data. The divergence in the simulations keeps the same sign with that of the reanalysis at the four time slices.

The success of the simulation in the large-scale variation of diurnal winds, and the associated diurnal phases of the divergence fields, explain why the models simulated the observed variation of stratiform rainfall. The ability of the CAM5 in simulating the maximum early-morning diurnal rainfall over the East China Sea is

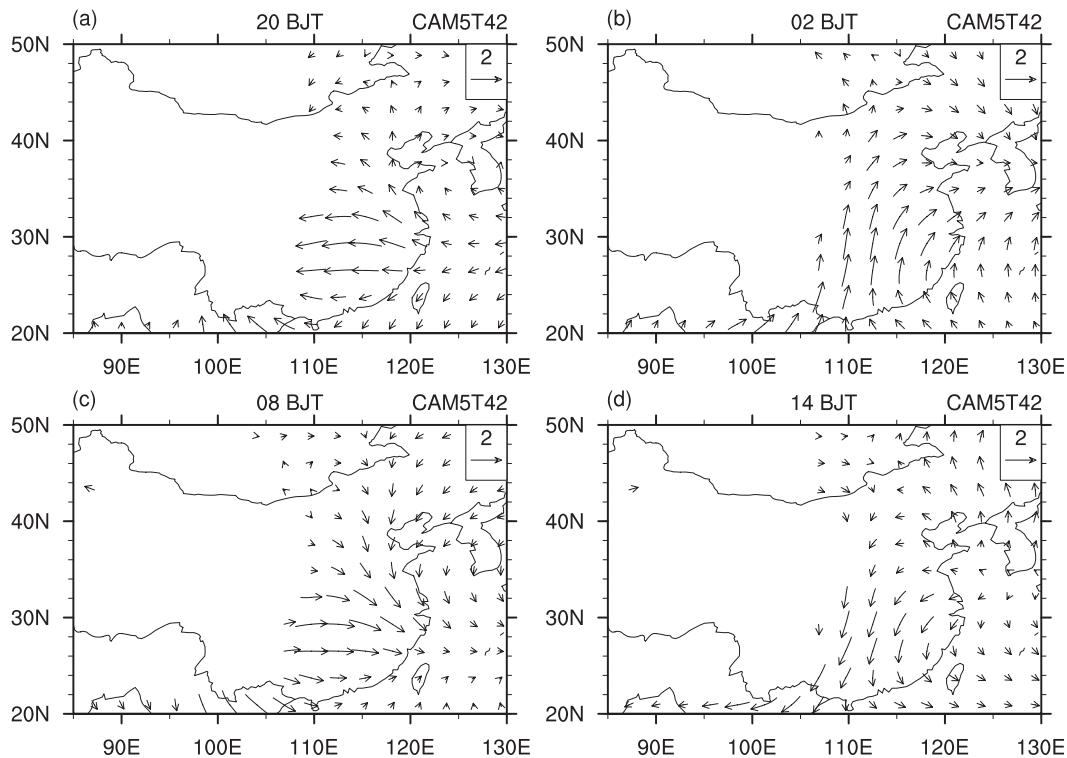


FIG. 8. As in Fig. 7 but for the coarse-resolution model.

therefore likely a consequence of the large-scale diurnal variation of the winds in that region.

6. Summary and conclusions

The performance of CAM5 with 2.8° and 0.5° horizontal resolution in simulating the summertime mean and diurnal cycle of precipitation and low-level circulation over subtropical East Asia has been assessed. The simulated diurnal rainfall is evaluated against corresponding results based on station rain gauge data, satellite observations, and reanalysis product. The physical cause of the model's ability has been investigated by analyzing the diurnal variation of rainfall with respect to its convective and stratiform components. New findings are summarized as follows.

- 1) CAM5 at both 2.8° and 0.5° resolution is capable of simulating the diurnal phase of the stratiform rainfall in East Asia in the summer season, with a midnight to early-morning maximum. This diurnal phase of stratiform rainfall is shown to be consistent with the diurnal variation of large-scale circulation, which is reasonably simulated in both models.
- 2) The convective rainfall in TRMM data, over the western plain, peaks in both early morning and late

afternoon, while it primarily peaks in late afternoon over the eastern plain. The models simulated a noon-time maximum of convective rainfall that occurs earlier and stronger over land than in observations. Over the ocean, the models simulated a convective maximum in early morning that is consistent with observations.

- 3) Superposition of the two types of rainfall can explain why the models simulated well the diurnal variation of total rainfall in some regions but not in other regions. Over the East China Sea, the models simulated the correct diurnal cycle of total rainfall with the maximum peak in early morning. This is because the stratiform rainfall and convective rainfall in the observation are in phase with each other in this region and the models simulated these phases correctly. In the western plain, the models simulated a much smaller diurnal magnitude of total rainfall than observation. This is because they simulated an out-of-phase relationship between convective and stratiform precipitation due to the missing nocturnal convective maximum in simulations. In the eastern plain, the models simulated a too strong noontime peak in total rainfall because convective rainfall is dominate in the models but not in observations.

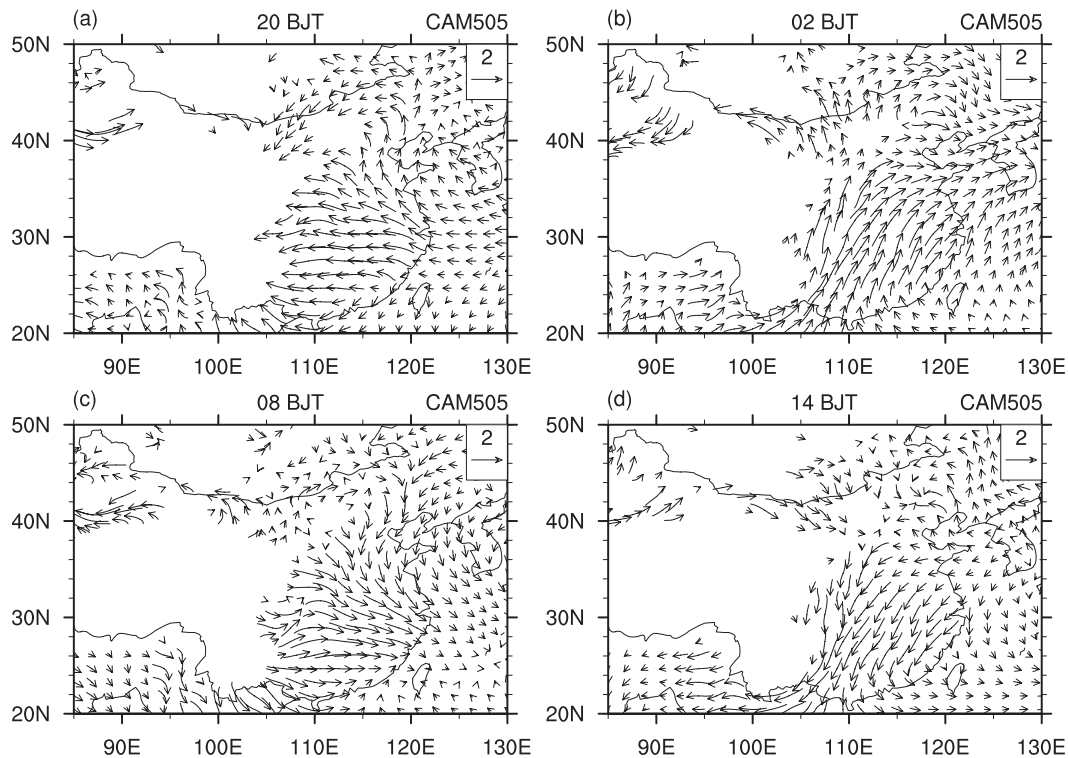


FIG. 9. As in Fig. 7 but for the fine-resolution model.

- 4) The high-resolution model simulated a better distribution of mean rainfall than the lower-resolution model, but it does not improve the diurnal variation of convective precipitation.
- 5) Over the Tibetan Plateau, diurnal maximum of total rainfall occurs in evening in the rain gauge data and at midnight in the satellite data, reflecting differences of measurements in valleys and over mountains. The models all simulated a late-afternoon maximum with amplitude smaller than that in the observations.

These results help us to understand the reasons why the models can simulate the diurnal rainfall in some regions but not in other regions. They point to the need of improving the convective parameterizations in the model so that the diurnal maximum can be delayed. Additionally, although we have shown some improvement in representation of the mean and diurnal rainfall with higher resolution, the high-resolution model suffers from very similar biases as in the coarse-resolution model. The inability to properly reproduce the regional characteristics in the diurnal amplitude and phase is

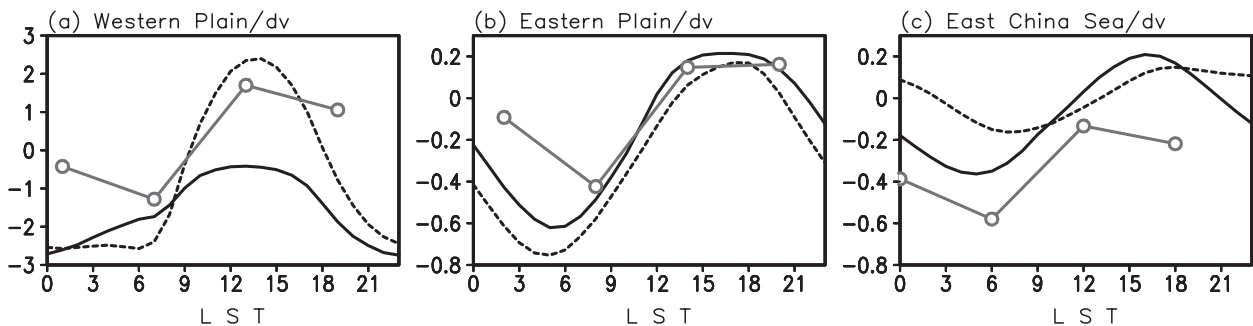


FIG. 10. Diurnal variations of the divergence (10^{-6} s^{-1}) derived from the coarse-resolution model (black solid lines), the fine-resolution model (black dashed lines), and the CFSR reanalysis (lines with circles) averaged in (a) the western plain, (b) the eastern plain, and (c) East China Sea. The x axis is LST.

primarily due to the problems in the model physics that are largely unrelated to resolution.

Acknowledgments. This research is supported by the Major National Basic Research Program of China (973 Program) on Global Change under Grants 2010CB951902 and 2010CB951802 and the National Natural Science Foundation of China under Grants 41205053 and 41221064. Additional supported is provided by the National Science Foundation, the Office of Sciences of the Department of Energy, and NASA to Stony Brook University. Wuyin Lin is supported by the Office of Sciences of the U.S. Department of Energy through the FASTER project to Brookhaven National Laboratory.

REFERENCES

- Andersson, T., 1970: The diurnal variation of precipitation frequency over Weather Ship M. *J. Appl. Meteor.*, **9**, 17–19.
- Arakawa, O., and A. Kitoh, 2005: Rainfall diurnal variation over the Indonesian maritime continent simulated by 20 km-mesh GCM. *SOLA*, **1**, 109–112.
- Betts, A. K., and C. Jakob, 2002a: Study of diurnal cycle of convective precipitation over Amazonia using a single column model. *J. Geophys. Res.*, **107**, 4732, doi:10.1029/2002JD002264.
- , and —, 2002b: Evaluation of the diurnal cycle of precipitation, surface thermodynamics, and surface fluxes in the ECMWF model using LBA data. *J. Geophys. Res.*, **107**, 8045, doi:10.1029/2001JD000427.
- Boyle, J., and S. A. Klein, 2010: Impact of horizontal resolution on climate model forecasts of tropical precipitation and diabatic heating for the TWP-ICE period. *J. Geophys. Res.*, **115**, D23113, doi:10.1029/2010JD014262.
- Bretherton, C. S., and S. Park, 2009: A new moist turbulence parameterization in the Community Atmosphere Model. *J. Climate*, **22**, 3422–3448.
- Chen, G., W. Sha, and T. Iwasaki, 2009: Diurnal variation of precipitation over southeastern China: Spatial distribution and its seasonality. *J. Geophys. Res.*, **114**, D13103, doi:10.1029/2008JD011103.
- Chen, H., W. Yuan, J. Li, and R. Yu, 2012: A possible cause for different diurnal variations of warm season rainfall as shown in station observations and TRMM 3B42 data over the southeastern Tibetan Plateau. *Adv. Atmos. Sci.*, **29**, 193–200.
- Collier, J. C., and K. P. Bowman, 2004: Diurnal cycle of tropical precipitation in a general circulation model. *J. Geophys. Res.*, **109**, D17105, doi:10.1029/2004JD004818.
- Collins, W. D., and Coauthors, 2004: Description of the NCAR Community Atmosphere Model (CAM 3.0). NCAR Tech. Note NCAR/TN-464+STR, 226 pp.
- , and Coauthors, 2006: The Community Climate System Model version 3 (CCSM3). *J. Climate*, **19**, 2122–2143.
- Cook, A. W., 1939: The diurnal variation of summer rainfall at Denver. *Mon. Wea. Rev.*, **67**, 95–98.
- Dai, A., 2001: Global precipitation and thunderstorm frequencies. Part II: Diurnal variations. *J. Climate*, **14**, 1112–1128.
- , 2006: Precipitation characteristics in eighteen coupled climate models. *J. Climate*, **19**, 4605–4630.
- , and K. E. Trenberth, 2004: The diurnal cycle and its depiction in the Community Climate System Model. *J. Climate*, **17**, 930–951.
- Donner, L. J., and V. T. Phillips, 2003: Boundary layer control on convective available potential energy: Implications for cumulus parameterization. *J. Geophys. Res.*, **108**, 4701, doi:10.1029/2003JD003773.
- Duffy, P. B., B. Govindasamy, J. P. Iorio, J. Milovich, K. R. Sperber, K. E. Taylor, M. F. Wehner, and S. L. Thompson, 2003: High-resolution simulations of global climate, part 1: Present climate. *Climate Dyn.*, **21**, 371–390.
- Fu, Y., and G. Liu, 2007: Possible misidentification of rain type by TRMM PR over Tibetan Plateau. *J. Appl. Meteor. Climatol.*, **46**, 667–672.
- Gettelman, A., and Coauthors, 2010: Global simulations of ice nucleation and ice supersaturation with an improved cloud scheme in the Community Atmosphere Model. *J. Geophys. Res.*, **115**, D18216, doi:10.1029/2009JD013797.
- Gray, W. M., and R. W. Jacobson, 1977: Diurnal variation of deep cumulus convection. *Mon. Wea. Rev.*, **105**, 1171–1188.
- Hamilton, K., 1981: Latent heat release as a possible forcing mechanism for atmospheric tides. *Mon. Wea. Rev.*, **109**, 3–17.
- Hara, M., T. Yoshikane, H. G. Takahashi, F. Kimura, A. Noda, and T. Tokioka, 2009: Assessment of the diurnal cycle of precipitation over the maritime continent simulated by a 20 km mesh GCM using TRMM PR data. *J. Meteor. Soc. Japan*, **87A**, 413–424.
- Huffman, G. J., and Coauthors, 2007: The TRMM Multisatellite Precipitation Analysis (TMPA): Quasi-global, multiyear, combined-sensor precipitation estimates at fine scales. *J. Hydrometeorol.*, **8**, 38–55.
- Iacono, M. J., J. S. Delamere, E. J. Mlawer, M. W. Shephard, S. A. Clough, and W. D. Collins, 2008: Radiative forcing by long-lived greenhouse gases: Calculations with the AER radiative transfer models. *J. Geophys. Res.*, **113**, D13103, doi:10.1029/2008JD009944.
- Iguchi, T., T. Kozu, R. Meneghini, J. Awaka, and K. Okamoto, 2000: Rain-profiling algorithm for the TRMM precipitation radar. *J. Appl. Meteor.*, **39**, 2038–2052.
- Kikuchi, K., and B. Wang, 2008: Diurnal precipitation regimes in the global tropics. *J. Climate*, **21**, 2680–2696.
- Kraus, E. B., 1963: The diurnal precipitation change over the sea. *J. Atmos. Sci.*, **20**, 551–556.
- Kummerow, C., and Coauthors, 2001: The evolution of the Goddard profiling algorithm (GPROF) for rainfall estimation from passive microwave sensors. *J. Appl. Meteor.*, **40**, 1801–1820.
- Lee, M.-I., and Coauthors, 2007a: An analysis of the warm-season diurnal cycle over the continental United States and northern Mexico in general circulation models. *J. Hydrometeorol.*, **8**, 344–366.
- , and Coauthors, 2007b: Sensitivity to horizontal resolution in the AGCM simulations of warm season diurnal cycle of precipitation over the United States and northern Mexico. *J. Climate*, **20**, 1862–1881.
- Lin, X., D. A. Randall, and L. D. Fowler, 2000: Diurnal variability of the hydrologic cycle and radiative fluxes: Comparisons between observations and a GCM. *J. Climate*, **13**, 4159–4179.
- Morrison, H., and A. Gettelman, 2008: A new two-moment bulk stratiform cloud microphysics scheme in the Community Atmosphere Model, version 3 (CAM3). Part I: Description and numerical tests. *J. Climate*, **21**, 3642–3659.
- , J. A. Curry, and V. I. Khvorostyanov, 2005: A new double-moment microphysics parameterization for application in cloud and climate models. Part I: Description. *J. Atmos. Sci.*, **62**, 1665–1677.

- Neale, R. B., J. H. Richter, and M. Jochum, 2008: The impact of convection on ENSO: From a delayed oscillator to a series of events. *J. Climate*, **21**, 5904–5924.
- , and Coauthors, 2010: Description of the NCAR Community Atmosphere Model (CAM 5.0). NCAR Tech. Note NCAR/TN-486+STR, 283 pp.
- Nesbitt, S. W., and E. J. Zipser, 2003: The diurnal cycle of rainfall and convective intensity according to three years of TRMM measurements. *J. Climate*, **16**, 1456–1475.
- Oki, T., and K. Musiake, 1994: Seasonal change of the diurnal cycle of precipitation over Japan and Malaysia. *J. Appl. Meteor.*, **33**, 1445–1463.
- Park, S., and C. S. Bretherton, 2009: The University of Washington shallow convection and moist turbulence schemes and their impact on climate simulations with the Community Atmosphere Model. *J. Climate*, **22**, 3449–3469.
- Ploshay, J. J., and N.-C. Lau, 2010: Simulation of the diurnal cycle in tropical rainfall and circulation during boreal summer with a high-resolution GCM. *Mon. Wea. Rev.*, **138**, 3434–3453.
- Randall, D. A., Harshvardhan, and D. A. Dazlich, 1991: Diurnal variability of the hydrologic cycle in a general circulation model. *J. Atmos. Sci.*, **48**, 40–62.
- Raymond, D. J., and A. M. Blyth, 1986: A stochastic mixing model for non-precipitating cumulus clouds. *J. Atmos. Sci.*, **43**, 2708–2718.
- , and —, 1992: Extension of the stochastic mixing model to cumulonimbus clouds. *J. Atmos. Sci.*, **49**, 1968–1983.
- Saha, S., and Coauthors, 2010: The NCEP Climate Forecast System Reanalysis. *Bull. Amer. Meteor. Soc.*, **91**, 1015–1057.
- Sato, T., H. Miura, M. Satoh, Y. N. Takayabu, and Y. Q. Wang, 2009: Diurnal cycle of precipitation in the tropics simulated in a global cloud-resolving model. *J. Climate*, **22**, 4809–4826.
- Sorooshian, S., X. Gao, K. Hsu, R. A. Maddox, Y. Hong, H. V. Gupta, and B. Imam, 2002: Diurnal variability of tropical rainfall retrieved from combined GOES and TRMM satellite information. *J. Climate*, **15**, 983–1001.
- Tao, S. Y., and L. X. Chen, 1987: A review of recent research on the East Asian summer monsoon. *Monsoon Meteorology*, C. P. Chang and T. N. Krishnamurti, Eds., Oxford University Press, 60–92.
- Wallace, J. M., 1975: Diurnal variations in precipitation and thunderstorm frequency over the conterminous United States. *Mon. Wea. Rev.*, **103**, 406–419.
- Xie, S., and M. H. Zhang, 2000: Impact of the convection triggering function on single-column model simulations. *J. Geophys. Res.*, **105** (D11), 14 983–14 996.
- , and Coauthors, 2002: Intercomparison and evaluation of cumulus parametrizations under summertime midlatitude continental conditions. *Quart. J. Roy. Meteor. Soc.*, **128**, 1095–1135.
- Yang, G. Y., and J. Slingo, 2001: The diurnal cycle in the tropics. *Mon. Wea. Rev.*, **129**, 784–801.
- Yin, S. Q., D. L. Chen, and Y. Xie, 2009: Diurnal variations of precipitation during the warm season over China. *Int. J. Climatol.*, **29**, 1154–1170.
- Yu, R., T. Zhou, A. Xiong, Y. Zhu, and J. Li, 2007: Diurnal variations of summer precipitation over contiguous China. *Geophys. Res. Lett.*, **34**, L01704, doi:10.1029/2006GL028129.
- Yuan, W., R. Yu, M. Zhang, W. Lin, H. Chen, and J. Li, 2012: Regimes of diurnal variation of summer rainfall over subtropical East Asia. *J. Climate*, **25**, 3307–3320.
- Zhang, G. J., 2003: Roles of tropospheric and boundary layer forcing in the diurnal cycle of convection in the U.S. southern great plains. *Geophys. Res. Lett.*, **30**, 2281, doi:10.1029/2003GL018554.
- , and N. A. McFarlane, 1995: Sensitivity of climate simulations to the parameterization of cumulus convection in the Canadian Climate Centre general circulation model. *Atmos.–Ocean*, **33**, 407–407.
- Zhou, T., R. Yu, X. Liu, Y. Guo, Y. Yu, and X. Zhang, 2005: Atmospheric water vapor transport associated with typical anomalous summer rainfall patterns in China. *J. Geophys. Res.*, **110**, D08104, doi:10.1029/2004JD005413.
- , —, H. Chen, A. Dai, and Y. Pan, 2008: Summer precipitation frequency, intensity, and diurnal cycle over China: A comparison of satellite data with rain gauge observations. *J. Climate*, **21**, 3997–4010.